

Creep failure of honeycombs made by rapid prototyping

P. E. Seiler^a, H. C. Tankasala^a, N. A. Fleck^{a,*}

^aDepartment of Engineering, University of Cambridge, Cambridge CB2 1PZ, United Kingdom

Abstract

Additive manufacture and rapid prototyping are versatile methods for the generation of lattice materials for applications in the creep regime. However, these techniques introduce defects that can degrade the macroscopic strength. In the present study, the in-plane tensile response of PMMA lattices is measured in the visco-plastic regime: tests are performed at 100 °C which is slightly below the glass transition temperature T_g of PMMA. Both *as-manufactured* defects (Plateau borders and strut thickness variation) and *as-designed* defects (missing cell walls, solid inclusions, and randomly perturbed joints) are introduced. The dispersion in macroscopic strength is measured for relative densities in the range of 0.07 to 0.19. It is observed that initial failure of the lattice is diffuse in nature, occurs at a number of uncorrelated locations, and is followed by the development of a single macroscopic crack transverse to the loading direction. In contrast, the same PMMA lattice fails in a correlated, brittle manner at room temperature. An FE study is performed to gain insight into the diffusive failure mode and the role played by *as-manufactured* defects, including the dispersion in tensile strength of individual struts of the lattice. A high damage tolerance to *as-designed* defects is observed experimentally: there is negligible knock-down in strength due to the removal of cell walls or to the presence of solid inclusions. These findings can aid the guide the design and manufacture of damage tolerant lattices in the creep regime.

Keywords: lattice materials, visco-plastic, tensile strength, rapid prototyping

*Corresponding author

Email addresses: pes34@cam.ac.uk (P. E. Seiler), hct30@cam.ac.uk (H. C. Tankasala), naf1@eng.cam.ac.uk (N. A. Fleck)

1. Introduction

Foams and lattices are increasingly used in engineering applications due to advances in additive manufacturing methods. There is a need to develop tough, stiff, and lightweight lattices, with high creep resistance for high temperatures applications, e. g. heat exchangers, thermal insulation and catalytic converters [1]. Whilst the creep behaviour of foams has been reported [2–11], few studies detail the tensile response of rate-sensitive, visco-plastic lattices [3, 12]. The present study addresses this gap in the literature, especially in regard to as-manufactured and as-designed imperfections and the implication of these two classes of imperfection on the macroscopic response. The present study is companion to the recent paper [13] on the brittle response of polymethyl methacrylate (PMMA) lattices tested at room temperature. In the present study, the defect-sensitivity of creep strength is compared with the defect-sensitivity of brittle strength as taken from [13], for the same geometries and same manufacturing technique.

1.1. Hexagonal lattices

A regular two-dimensional (2D) hexagonal lattice is shown in Fig. 1(b). It comprises struts of length ℓ and in-plane thickness t such that, for $t/\ell < 0.2$, the relative density of the lattice is given by

$$\bar{\rho} = \frac{2}{\sqrt{3}} \frac{t}{\ell} \quad (1)$$

as derived in [1]. Under macroscopic loading, the hexagonal lattice is bending-dominated [1]. Consequently, the macroscopic properties are sensitive to the value of $\bar{\rho}$. For example, consider the linear elastic response of a hexagonal lattices; the macroscopic stiffness E and the macroscopic strength σ_f^∞ scale with relative density according to

$$E = \frac{3}{2} \bar{\rho}^3 E_s \quad \text{and} \quad \sigma_f^\infty = \frac{1}{3} \bar{\rho}^2 \sigma_{fs} \quad (2)$$

in terms of the stiffness E_s and strength σ_{fs} of the parent solid. In the present study we select polymethyl methacrylate (PMMA) as the cell wall material of the hexagonal lattices since it behaves in an elastic-brittle manner at room temperature, but exhibits a visco-plastic characteristic at temperatures close to the glass

transition temperature, T_g .

The presence of as-manufactured defects significantly degrade the macroscopic tensile response of elastic-brittle hexagonal lattices [13]. For example, a dispersion in strut thickness and in tensile strength of individual struts within the lattice led to a knock-down in the mean macroscopic strength. Successive strut failure occurs in the vicinity of a previously failed strut, and this leads to a correlated failure mode. Ultimately, a single macroscopic crack nucleates and advances from one edge of the lattice. This failure mechanism was predicted by assuming a local tensile strain failure criterion. Furthermore, both the measured and predicted macroscopic strength of a lattice of finite specimen geometry agree with the predictions of Gibson and Ashby [1]. The strength of the brittle lattice is sensitive to the presence of *as-manufactured* defects in the form of missing cell walls¹, whereas the strength of the lattice is relatively insensitive to the presence of *as-designed* defects in the form of randomly misplaced joints and filled cells. The aim of the present study is to determine whether similar conclusions can be drawn for a lattice deforming in the creep regime. For example, is the degree of imperfection sensitivity in the creep regime significantly less than that in the elastic-brittle regime due to damage being more diffuse in nature?

1.2. The creep response of foams and honeycombs

At elevated temperature (T close to T_g for polymers or T exceeding 30% of the absolute melting temperature for metals and ceramics), foams undergo time-dependent plastic flow, or *creep*. Gibson and Ashby [1] have considered the case of a foam with cell walls that undergo power-law creep, such that the uniaxial strain rate $\dot{\epsilon}$ of the solid scales with the tensile stress σ according to

$$\dot{\epsilon} = \dot{\epsilon}_{0s} \left(\frac{\sigma}{\sigma_{0s}} \right)^{n_s} \quad (3)$$

in terms of the material constants $\dot{\epsilon}_{0s}$, σ_{0s} , and creep exponent n_s . The creep exponent of the honeycombs or foams inherits the value n_s from that of the parent solid, as explained by Boccaccini et al. [14]. The remote

¹The removal of cell walls leads to a shift in behaviour from strength control to K -dominated behaviour at a small transition flaw size a_T on the order of 1 cell size.

creep solid $\dot{\epsilon}^\infty$ of an open-cell foam scales with the macroscopic tensile stress σ^∞ according to

$$\frac{\dot{\epsilon}^\infty}{\dot{\epsilon}_{0s}} = \frac{0.6}{(n_s + 2)} \left(\frac{1.7(2n_s + 1)}{n_s} \frac{\sigma^\infty}{\sigma_{0s}} \right)^{n_s} \left(\frac{1}{\bar{\rho}} \right)^{(3n_s+1)/2} \quad (4)$$

The dependence of creep rate upon relative density, as stated in Eq. (4), has been confirmed experimentally for open-cell metallic [2] and ceramic foams [11]. As for metallic foams, the creep parameters of polymeric foams inherit their values from those of the parent solid, for example, Huang and Gibson [9] found that the creep activation energy of foamed polystyrene equals that of the solid. The visco-elastic response of open and closed-celled polymer foams has been studied in the low-temperature regime [4–6, 9] whereas the present study addresses the high-temperature visco-plastic, creep response of polymer honeycombs at temperatures close to T_g .

It is broadly accepted that the power-law creep response of honeycombs and foams is sensitive to the presence of missing cell walls [10, 15], to a dispersion in cell wall thickness [16], and to the existence of randomly misplaced joints [16], and Plateau borders [12, 17]. The emphasis of the present study differs from previous work: our aim is to explore the sensitivity of failure mechanisms (localised versus diffuse), and associated strength and ductility, to the presence of geometric and material imperfections.

1.3. Scope of study

The purpose of the current study is to examine experimentally the deformation and fracture responses of two-dimensional (2D), visco-plastic, hexagonal honeycombs made by rapid prototyping. The honeycombs were cut from polymethyl methacrylate (PMMA) sheets and the macroscopic stress versus strain response was measured for uniaxial tension at fixed strain rate, in a temperature-controlled chamber at 100 °C which is close to the glass transition temperature T_g of PMMA. The as-manufactured lattice geometry contains Plateau borders and strut thickness variation, and the magnitude of these 2 defects was measured by computer-assisted tomography (CT). Finite element (FE) predictions of the macroscopic stress versus strain response were made by assuming (i) the geometry of the CT-scans, (ii) the measured visco-plastic response of a single strut, and (iii) a dispersion of strut by strut ductility due to variations in the thermal history of the struts during manufacture.

The notion of a transition flaw size is used to quantify the sensitivity of lattice strength to defect size. Irregular lattices were also created by the introduction of as-designed defects, specifically a centre crack (due to missing cell walls), solid inclusions in the form of filled cells, and randomly perturbed joints. The knock-down in lattice strength due to each of these defects was measured.

2. Experimental investigation

The experimental procedure, including the manufacturing parameters for laser-cutting the PMMA sheets, has already been detailed in the companion study [13]. The same manufacturing routine was applied in this study using the same material batch of cast 5 mm thick PMMA sheets. In brief, specimens were manufactured by laser-cutting² into the following 5 geometries:

- (i) single strut specimen, as shown in Fig. 1(a), for material characterisation on a small scale;
- (ii) regular hexagonal lattice, as shown in Fig. 1(b), to measure the lattice response, absent as-designed defects;
- (iii) irregular hexagonal lattice containing as-designed defects in the form of (a) randomly perturbed joints, (b) missing cell walls, or (c) solid inclusions, see Fig. 2.

The dispersion in strut by strut thickness t and in Plateau border radius r in of lattice specimens of type (ii) and (iii) have already been characterised by X-ray computed tomography (CT) in Ref. [13]. Both t and r are defined in Fig. 1(b). The strut thickness was measured at mid-length of 453 struts. It follows a normal distribution with a mean value $\bar{t} = 0.47$ mm, where the overbar throughout this study denotes the average value, with the exception of the relative density. The standard deviation of the strut thickness is $t_{sd} = 0.09$ mm. The Plateau border radius was quantified by a measured mean value of $\bar{r} = 0.4$ mm and standard deviation $r_{sd} = 0.1$ mm. For lattice specimens of type (ii), the relative density of the lattice $\bar{\rho}$ is varied from 0.07 to 0.19 by varying strut length ℓ in the range of 3.0 mm to 7.5 mm, as demanded by Eq. (1). The PMMA material employed in this study has a glass transition temperature³ $T_g = 385$ K. All specimens were tested at $T = 100$ °C = $0.97 T_g$.

²HPC Laser Ltd LS6090 Pro 80 Watt laser cutter; process parameters: cutting speed, 60% power, 55% corner power.

³The value of T_g was measured by Dynamic Mechanical Analysis (DMA) of a single PMMA cantilever beam at an excitation frequency

3. Manufacture of lattice specimens and test method

A computer-aided drawing (CAD) of the geometry of a regular hexagonal lattice, as shown in Fig. 1(b), was created using the *OpenSCAD* software.⁴ This CAD file provides an input to the laser cutting machine with sufficient data to define the translation of the cutting head relative to a fixed position on the PMMA sheet.

The hexagonal lattices were manufactured to dogbone shape in order to ensure that failure occurs within the gauge section, see Fig. 1(b). All lattice specimens have a gauge width $W = 11\sqrt{3}\ell$ (or 11 cells) and a gauge length $L = 11\ell$ (or 7 cells).

The front and back faces of the end, gripping portions of the lattice specimens were adhered to 2 mm thick aluminium alloy end tabs, see Fig. 1(b). All lattice specimens were tested in uniaxial tension using a servo hydraulic test machine at a nominal strain rate of $\dot{\epsilon} = 4 \times 10^{-4} \text{ s}^{-1}$. The tests were conducted at 100 °C in a temperature-controlled chamber with a glass window for in-situ observation of the specimen during the test. The temperature was maintained to a precision of $\Delta T \pm 2 \text{ K}$ during each test. The load P was measured via a load cell clamped to the stationary platen of the rig while the extension u of the gauge length was determined by Digital Image Correlation (DIC), as described in Ref. [13]. Prior to the start of each test, the lattice specimens were coated with a thin layer of white chalk and a speckle pattern was generated by the spraying of black paint in order to enhance the contrast of the DIC imagery. A digital camera⁵ was used to track facets of size 20×20 pixels in the vicinity of all nodes. A Matlab script was applied for sub-pixel tracking of the nodal displacement. The axial strain of each strut was thereby measured in the gauge section of the specimens, and the axial failure strain e_f of each strut was recorded.

4. Material characterisation

The as-manufactured material properties of solid PMMA were measured from the tensile response of laser-cut single strut specimens of mean strut thickness $\bar{t} = 0.47 \text{ mm}$ and strut length $L_s = 10 \text{ mm}$. The tests were conducted at 100 °C in a temperature-controlled chamber as described before. The extension of the single

equal to 0.1 Hz and a heating rate of 5 °C/min, refer to [18] for details of the test procedure.

⁴<https://www.openscad.org>

⁵maximum resolution: 4608 × 3288 pixels, 55 mm lens for lattices and 100 mm lens for single strut tests

strut specimens was measured by optical tracking of white dots at the ends of the gauge length along the centre-line of the specimen by DIC.

The measured nominal stress versus nominal strain response for 3 different strain rates within the range $4 \times 10^{-4} \text{ s}^{-1}$ to $4 \times 10^{-3} \text{ s}^{-1}$ are shown in Fig. 3. The flow strength increases with increasing strain rate. Negligible necking was found at 100°C due to the visco-plastic material behaviour which is in agreement with the observations of Van Loock and Fleck [18]. The single strut failure strain ε_{fs} is insensitive to strain rate over the range tested. The stress versus strain data and the nominal single strut failure strain of $\bar{\varepsilon}_{\text{fs}} = 2.5$ were used for modelling purposes in Section 6.

5. Measured tensile response of as-manufactured lattice specimens

The measured macroscopic nominal stress σ^∞ versus nominal strain ε^∞ responses of 3 lattice specimens of Fig. 1(b) are shown in Fig. 4(a). Representative curves are shown for one specimen at each relative density of 0.07, 0.11, and 0.19. The macroscopic quantities σ^∞ and ε^∞ are defined in terms of the measured force P on the top edge and the extension u of the gauge length as $\sigma^\infty = P/(WB_0)$ and $\varepsilon^\infty = u/L$, respectively. The dimensions (W, L) are defined in Fig. 1(b); $W = 96 \text{ mm}$, $L = 55 \text{ mm}$, and $B_0 = 5 \text{ mm}$.

The sequence of strut failure in lattice specimen of $\bar{\rho} = 0.11$ is shown in Fig. 4(a) with the corresponding locations of strut failure marked in Fig. 4(b). The following observations are made from Fig. 4(a) and (b); these features remain consistent across all the specimens tested in this study. All failed struts exist within the gauge section of the specimen and strut failure occurs always close to a joint. First strut failure does not necessarily occur at the edge of the specimen. Subsequent strut failures occur at random locations, leading to a diffuse mode of damage, see for example Fig. 4(b). First strut failure is accompanied by only a small drop in the load P (and in turn σ^∞). The cell wall solid has a sufficiently high strain-rate hardening response that σ^∞ is almost constant during the progressive failure of the first 6 struts at random locations within the lattice. Approximately 54% of the failed struts are inclined at $\pm 60^\circ$ to the loading axis in the undeformed configuration. This observation is in contrast to the behaviour of elastic-brittle PMMA lattices wherein 90% of the failed struts were inclined at $\pm 60^\circ$ to the loading axis [13].

It is instructive to compare the strut nominal ductility e_f with the nominal failure strain of the cell wall solid $\bar{\epsilon}_{fs}$, as follows. Denote e_f as the fractional change in the node-to-node distance of the failed strut (see inset in Fig. 5). The measured values of e_f are plotted in Fig. 5 for increasing values of ϵ^∞ for 3 lattice specimens of each relative density of Fig. 4(a), with the ordinate in each case normalised by the nominal solid ductility $\bar{\epsilon}_{fs} = 2.5$. A large scatter in e_f is noted for all values of $\bar{\rho}$ considered in this study, with e_f approaching the value of $\bar{\epsilon}_{fs}$ at macroscopic strains larger than 80%.

6. Simulations

6.1. Details of the FE model

The finite element (FE) method is used to investigate numerically the tensile response of PMMA lattices made from rapid prototyping. The main objectives of the FE study are to (i) examine the sensitivity of the macroscopic response to as-manufactured defects such as variation in strut thickness and Plateau border radius, (ii) identify the factors that lead to large macroscopic ductility (up to 100% before final fracture) along with the diffuse mode of fracture as observed in the experiments, and (iii) propose design criteria for lattices of high defect tolerance.

Two geometries of the lattice specimens of relative density $\bar{\rho} = 0.11$ are modelled explicitly for comparison with the experimental observations: (i) an ideal lattice with constant strut thickness and constant Plateau border radius, and (ii) structural realisations of the as-manufactured lattice, as shown in Fig. 6, for direct comparison with the experimental observations. The specimen geometry was scanned by CT and the FE mesh was constructed using the centre plane of the scanned geometry. Quasi-static calculations are performed within ABAQUS/Explicit v6.14 to simulate the deformation and failure response of these specimens under remote uniaxial tensile loading.

6.1.1. Geometry and loading

The as-manufactured lattice of Fig. 6 contains a total of 453 struts, each of length $\ell \approx 5$ mm. A typical unit cell within the lattice is shown in the inset of Fig. 6: the struts within the lattice have a variable thickness, with a mean value across the sample $\bar{t} = 0.47$ mm and standard deviation $t_{sd}/\bar{t} = 0.19$ such that the average relative

density of the lattice is $\bar{\rho} = 0.11$. The FE mesh for this lattice comprises quadratic triangular elements in plane strain (type CPE6M) of uniform size ℓ_e chosen to be such that the thinnest strut in the lattice has at least five elements across its thickness, and the stress concentration at the Plateau borders is adequately captured, as shown in the insert of Fig. 6.

The uniaxial loading on the specimen is simulated by constraining all the degrees of freedom along the bottom edge of the specimen while the top edge is displaced in the x_2 -direction of the specimen, see Fig. 6. The response is compared in terms of the load P versus applied displacement u for the single strut specimens and in terms of the macroscopic variables, nominal stress σ^∞ and the nominal strain ε^∞ for the lattice, defined as follows: $\varepsilon^\infty = u/L$ and $\sigma^\infty = P/(WB_0)$, where the gauge dimensions, length L and width W , are as denoted in Fig. 6(a) and B_0 is the out-of-plane thickness of the specimen.

6.1.2. Material model

The cell wall material is modelled as an elastic, visco-plastic solid. Tensile fracture of the individual struts of the lattice is simulated using an idealised Johnson-Cook type continuum damage mechanics approach. This approach assumes the initiation of damage based on a local strain criterion, and its evolution based on a prescribed work of fracture. A detailed explanation of the material model assumed in the FE simulations is given below.

The initial response of the cell wall is linear elastic with solid Young's modulus $E_S = 400$ MPa and Poisson's ratio $\nu_S = 0.3$, as taken from the measured values for the single strut specimens. We adopt a visco-plastic constitutive law in terms of the true plastic strain ε^P , true stress σ , and strain rate $\dot{\varepsilon}$. It has the form

$$\sigma = \sigma_0 \sinh^{-1} \left(\frac{\dot{\varepsilon}}{\dot{\varepsilon}_0} \right) f(\varepsilon^P) \quad (5)$$

where the reference values $(\sigma_0, \dot{\varepsilon}_0)$ are taken as $\sigma_0 = 1$ MPa and $\dot{\varepsilon}_0 = 4.4 \times 10^{-6} \text{ s}^{-1}$ such that $\sigma(\dot{\varepsilon}, \varepsilon^P = 0) = \sigma_Y(\dot{\varepsilon})$ for the 3 values of strain rate $\dot{\varepsilon} = 4 \times 10^{-4} \text{ s}^{-1}$, 10^{-3} s^{-1} , and $4 \times 10^{-3} \text{ s}^{-1}$ as indicated in Fig. 3. It remains to specify $f(\varepsilon^P)$ in Eq. (5). A curve-fitting procedure is carried out on the measured σ versus ε^P data excluding the peak and the subsequent strain-softening, as shown by the dashed lines in Fig. 3. This procedure

results in the following functional form for $f(\varepsilon^P)$:

$$f(\varepsilon^P) = \begin{cases} \exp(0.9\varepsilon^P) & \text{for } 0 \leq \varepsilon^P < 0.6 \\ 0.8 \exp(1.2\varepsilon^P) & \text{for } 0.6 \leq \varepsilon^P < 0.92 \\ 0.5 \exp(1.8\varepsilon^P) & \text{for } \varepsilon^P \geq 0.92 \end{cases} \quad (6)$$

Following Johnson and Cook [19], it is assumed that damage at a material element (i.e. integration point) *initiates* when the maximum principal tensile strain at that point attains the solid tensile ductility, ε_{fs} , as indicated in Fig. 6(b). A deterministic value of strut ductility (i.e. true strain to failure), $\varepsilon_{fs} = 1.3$, is assumed for all struts in the lattice as taken from the measured mean ductility of single strut specimens, recall Fig. 3.

The subsequent *evolution* of damage at a material point is specified via a linear softening σ versus ε^P relationship given by

$$\sigma = \sigma_f \left(1 - \frac{\varepsilon^P - \varepsilon_{fs}}{\Delta\varepsilon} \right) \quad (7)$$

where σ_f is the stress level at $\varepsilon^P = \varepsilon_{fs}$ as given by Eq. (6), and $\Delta\varepsilon$ is the plastic strain increment over the softening portion of the response, see Fig. 6(b). The value of $\Delta\varepsilon$ follows from the specified work of fracture in the softening regime, Γ_f , and the characteristic length associated with the finite element, ℓ_c , as: $\Delta\varepsilon = 2\Gamma_f/\sigma_f\ell_c$. Note that $\ell_c = \ell_e/2$ for quadratic triangular finite elements. A value of $\Gamma_f = 2.5 \text{ kJ/m}^2$ is assumed in the current FE simulations upon making use of the Irwin relation $\Gamma_f = K_{IC}^2/E$ with $K_{IC} = 1 \text{ MPa}\sqrt{\text{m}}$ as taken from [20] and $E = 400 \text{ MPa}$ as obtained from the single strut experiments. It is noted that the specification of damage evolution via Eq. (7) in terms of the size of the finite element alleviates the problem of mesh dependence of the solution; refer to Ref. [21] for details.

6.2. FE predictions of the tensile response of as-manufactured lattice specimens

In order to quantify the role of the as-manufactured defects such as the variation in strut thickness and in Plateau border radius, FE simulations were performed on a theoretically perfect lattice of uniform strut thickness t , Plateau border radius r , and a deterministic value of cell wall ductility ε_{fs} . The predicted response of a perfect lattice specimen of relative density $\bar{\rho} = 0.11$ is shown in Fig. 7(a) for $t = \bar{t} = 0.47 \text{ mm}$ and

$r = \bar{r} = 0.4$ mm and a true strain $\varepsilon_{fs} = 1.3$ for all struts in the lattice. The measured response of one as-manufactured specimen of $\bar{\rho} = 0.11$ is included in Fig. 7(a) for comparison. We find from Fig. 7(a) that the initial stiffness of the lattice is accurately predicted by the perfect geometry, implying a negligible effect of the geometric imperfections on the elastic stiffness of the lattice. The first strut to fail, does so at a macroscopic strain of 0.76, which significantly exceeds the measured nominal strain at first strut failure of 0.18. The macroscopic strength of the lattice is also higher for the perfect lattice.

The sensitivity of the macroscopic strength to as-manufactured defects is explored by performing an FE simulation on the precise geometry of the as-manufactured specimen taken from a CT scan of the mid-plane section. This geometry contains a dispersion in strut thickness and in Plateau border radius as specified by $t_{sd}/\bar{t} = 0.19$ and $r_{sd}/\bar{r} = 0.25$, respectively. A deterministic value of cell wall ductility $\varepsilon_{fs} = 1.3$ is again assumed for all struts in the lattice such that $\varepsilon_{f,sd} = 0$. The predicted response of the as-manufactured specimen shows early strut failure at remote nominal strain of 0.42 and a macroscopic strength value somewhat higher than the measured value, see Fig. 7(a). The failure of struts in the FE simulations for both the perfect and as-manufactured geometries occurs in a correlated crack-like manner as shown in Fig. 7(b), suggesting a strong sensitivity to the scatter in strut ductility from the laser cutting process.

6.2.1. Effect of the spatial variation in ductility

Recall the variation in average failure strain e_f of all failed struts as shown in Fig. 5. These data are re-plotted in Fig. 8 in the form of a probability distribution curve $p(e_f)$. The best-fitting distribution of the measured values of e_f across all the lattice specimens is that of a Gaussian distribution with a mean value $e_f = 1.63$ and standard deviation $e_{sd}/\bar{e}_f = 0.4$. In order to assess the role of dispersion in strut ductility, FE simulations were performed on one realisation of the as-manufactured geometry, with a normal distribution of strut ductility ε_{fs} such that the mean value across 453 struts of the specimen is $\bar{\varepsilon}_f = 1.3$ and the standard deviation is $\varepsilon_{f,sd}/\bar{\varepsilon}_f = e_{sd}/\bar{e}_f = 0.4$.

The predicted macroscopic response of the as-manufactured lattice geometry with a dispersion in strut ductility is shown in Fig. 7(c); the measured response of this specimen is re-plotted here for comparison. We find from Fig. 7(c) that the dispersion in ductility at a strut level leads to the early failure of struts, consistent with

experimental observation. The first strut to fail is at the edge of the specimen, it fails at a nominal strain of $\varepsilon^\infty = 0.18$, and it is of thickness $t = 0.3$ mm and ductility $\varepsilon_{fs} = 1.03$. Subsequent strut failure in the FE simulation occurs at random locations within the lattice. The macroscopic strength has dropped to 30% of the value at first strut failure when the size of the cluster of failed struts approaches the half width of the specimen at $\varepsilon^\infty = 1$. The sequence and location of strut failure with $\varepsilon_{f,sd}/\bar{\varepsilon}_f = 0.4$ is shown in Fig. 7(b): the mode of damage is diffuse in nature, in close agreement with experimental observations.

The probability distribution $p(e_f)$ of e_f from 5 FE simulations (all performed with $\varepsilon_{f,sd}/\bar{\varepsilon}_f = 0.4$) is in excellent agreement with that of the measured distribution of ε_{fs} , see Fig. 8. The corresponding probability distribution of e_f for a deterministic value of strut ductility ($\bar{\varepsilon}_f = \varepsilon_f = 1.3$ and $\varepsilon_{f,sd} = 0$) is included in Fig. 8: an assumed variability in material failure strain clearly has a major influence upon the dispersion in strut ductility of the lattice.

6.3. Design for high defect tolerance

The transition flaw size is a useful parameter in quantifying the flaw sensitivity of a lattice. It can be interpreted as the minimum semi-length of crack for which catastrophic failure is dictated by the fracture toughness K_{IC}^∞ of the lattice rather than the tensile strength of the uncracked lattice. The notion of a transition flaw size was explored for the case of a brittle lattice by Fleck and co-workers ([13, 22, 23]) and for the case of a ductile lattice by Tankasala et al. [24]. In all cases, the transition flaw size a_T is given by

$$a_T \approx \frac{1}{\pi} \left(\frac{K_{IC}^\infty}{\sigma_f^\infty} \right)^2 \quad (8)$$

where K_{IC}^∞ is the macroscopic mode I fracture toughness of the lattice, and σ_f^∞ is the macroscopic tensile strength for a brittle lattice, or the macroscopic yield strength for a ductile lattice. The transition flaw size is on the order of one unit cell ($a_T \approx \ell$) for a brittle hexagonal lattice wherein a critical strut fails by bending. In contrast, for a ductile hexagonal lattice in which a critical strut fails by stretching, $a_T \approx 200\ell$, following the predictions of Tankasala et al. [24]. Consider the following 4 cases of lattice behaviour.

- (i) *Case A* is a brittle hexagonal lattice with a deterministic value of strut tensile strength (or ductility) such

that $\varepsilon_{f,sd} = 0$. A critical cell wall within the lattice fails by bending, giving rise to $a_T \approx \ell$. PMMA lattices at room temperature can behave in this manner, see for example, Seiler et al. [13].

- (ii) *Case B* is a ductile hexagonal lattice with a deterministic value of strut ductility ($\varepsilon_{f,sd} = 0$). When the failure of a cell wall is dictated by the average tensile strain across a section of the strut, then the transition flaw size of the lattice is on the order of few hundreds of cells, $a_T \approx 200\ell$ for a strain-hardening cell wall solid of $\varepsilon_{fs} = 0.1$ as previously reported by Tankasala et al. [24].
- (iii) *Case C* is a ductile hexagonal lattice with a dispersion in strut ductility such that $\varepsilon_{f,sd}/\bar{\varepsilon}_{fs} = 0.4$. Similar to case B, $a_T \approx 200\ell$ when the average tensile strain across a section of the strut dictates strut failure. The PMMA lattices of the current study (tested at 100°C) belong to this category.
- (iv) *Case D* is a brittle hexagonal lattice with a dispersion in strut tensile strength (or ductility) such that $\varepsilon_{f,sd}/\bar{\varepsilon}_{fs} = 0.4$. PMMA lattices at room temperature can also be of this class, and have the characteristic $a_T \approx \ell$, as confirmed recently by Seiler et al. [13].

Seiler et al. [13] have shown via experiments and FE simulations on finite PMMA lattices at room temperature that the mode of damage in brittle lattices of type A and D is correlated, as sketched in Fig. 10(a). A dispersion in the strut ductility leads to failure of struts at random locations within the lattice, but the transition flaw size $a_T \approx \ell$ dictates that the lattice fails catastrophically once 2 adjacent struts have failed. In contrast, we observe in the current study on PMMA lattices at high temperature (100°C) that the mode of damage, correlated versus diffuse, is sensitive to the value of $\varepsilon_{f,sd}/\bar{\varepsilon}_{fs}$. Consider, for example, case B with $\varepsilon_{f,sd}/\bar{\varepsilon}_{fs} = 0$. The transition flaw size for this case is $a_T \approx 200\ell$ for an *infinite* lattice. The lattices of the current study are of a finite width $W \approx 20\ell$. Consequently, catastrophic fracture of the specimen occurs when the length of the crack exceeds the minimum of $2a_T$ (given by Eq. (??)) and $0.5W$. The FE simulations of Fig. 7(c) confirm that correlated damage exists until catastrophic fracture of the specimen occurs when the length of the crack exceeds $0.5W$ (since $2a_T \approx 400\ell \gg W$), as sketched in Fig. 10(a). Alternatively, a high value of $\varepsilon_{f,sd}/\bar{\varepsilon}_{fs}$, such as $\varepsilon_{f,sd}/\bar{\varepsilon}_{fs} = 0.4$, leads to a diffuse mode of damage. Final fracture occurs when the size of a critical cluster of failed struts exceeds the least of $2a_T$ and $0.5W$; this is shown in case D of Fig. 10(a). The observed and predicted modes of

damage for all the above cases are summarised in a table in Fig. 10(a).

The damage tolerance of a lattice can be assessed, alternatively, by plotting the normalised macroscopic stress σ^∞ versus number of failed struts, n , across the width of the lattice. Here, $\bar{\sigma}_f^\infty$ is the mean macroscopic strength for first strut failure. Cases A through D are plotted in Fig. 10(b) and (c) from both the experiments and FE. The results for cases A and D are taken from Ref. [13], whereas cases B and C are from the present study. Recall that case C denotes a diffuse mode of strut failure and a large value of a_T . The macroscopic stress σ^∞ drops slightly with an increasing number n of failed struts, see (c). In contrast, the drop in σ^∞ with increasing n follows the net-section prediction, $\sigma^\infty/\bar{\sigma}_f^\infty = 1 - (n - 1)/(N - 1)$, for case B with a deterministic strut ductility ($\varepsilon_{fs,sd}/\bar{\varepsilon}_{fs} = 0$). Here N is the total number of struts in the gauge section; N equals 12 for this lattice specimen.

A sketch of the boundary between the correlated and diffuse modes of damage as a function of a_T/ℓ and $\varepsilon_{f,sd}/\bar{\varepsilon}_f$ is shown in Fig. 9(a) to indicate the parameter space of finite size lattices with high defect tolerance.

7. The effect of as-designed defects on macroscopic properties: experiment

Three types of macroscopic defect were introduced within the regular lattice by design: (i) misplaced joints, (ii) cells filled with solid inclusions, and (iii) missing cell walls. The resulting as-manufactured specimens contain geometric imperfections at the cell wall level (variation in strut thickness and Plateau border radius) in addition to one of the three macroscopic defects, see Fig. 2. The macroscopic tensile strength of the as-manufactured specimens was measured experimentally and then compared with that of the as-manufactured topologies designed without macroscopic defects. The sensitivity of measured tensile strength and failure strain to the presence of as-designed defects was thereby assessed.

7.1. Randomly perturbed joints

Randomly perturbed joints are introduced in the specimens to investigate the effect of cell wall misalignment. Imperfect hexagonal lattices were manufactured by generating a CAD file of a lattice with randomly perturbed joints. To achieve this, joints of a regular hexagonal lattice (of $\bar{\rho} = 0.11$) were repositioned randomly within a circular disc of radius R , following the procedure as used by Romijn and Fleck [25]. The degree of imperfection

was varied by selecting values of R/ℓ between 0 (regular lattice) and 0.5 (extremely imperfect lattice). A typical realisation of the as-manufactured lattice, for the choice $R/\ell = 0.5$, is shown in Fig. 2(a); only those joints which lie within the gauge section were misplaced. The random misplacement of the joints reduces the average strut length such that the relative density of the lattice increases by a factor of 1.0025 for $R/\ell = 0.1$ and by a factor of 1.0625 for $R/\ell = 0.5$, as previously noted by Romijn and Fleck [25]. This minor change in $\bar{\rho}$ is ignored in the current study.

The sensitivity to random perturbation of joints is measured for 2 macroscopic properties of the imperfect lattice: tensile strength σ_f^∞ and the tensile failure strain ε_f^∞ . These observed sensitivities are plotted in Fig. 10 as a function of the degree of imperfection R/ℓ , for the choice of $\bar{\rho} = 0.11$. The measured elastic-brittle response of hexagonal lattices from Seiler et al. [13] of the same relative density are included in Fig. 10. The ordinate in each case is normalised by its corresponding mean value as measured for the regular lattice ($R/\ell = 0$). Results are shown for 3 realisations of imperfect lattice for each choice of $R/\ell = 0, 0.3$, and 0.5.

No distinct knock-down in remote tensile strength and remote failure strain was found until $R/\ell \leq 0.3$. For $R/\ell = 0.5$, the scatter of strength and failure strain is drastically increased and a knock-down factor of 0.5 for strength and 0.6 for failure strain was found. In those samples, noticeable force chains are formed which lead to struts showing distinct stretching deformation which is responsible for the knock-down. The formation of force chains was predicted by Tankasala et al. [24] such that only a fraction of struts carry the macroscopic load. For brittle PMMA lattices at room temperature, the macroscopic tensile strength σ_f^∞ is almost insensitive to the value of R/ℓ .

The sequence of strut failure is shown in Fig. 10(c) for a representative specimen of $R/\ell = 0.5$. For each of the imperfect lattices considered in this study, first failure occurs in the centre of the specimens. Struts in the centre of specimens are more prone to fail at low remote strain for this sample class compared to regular lattices. After first strut failure, a diffusive failure mode was observed so that the nearest neighbours of an already failed strut do not necessarily fail next. Ronan et al. [26] found that this was the case for samples with randomly perturbed joints of lattices made out of elasto-plastic parent material. In contrast, neighbouring struts fail subsequent to initial strut failure in lattices with perturbed joints at room temperature.

7.2. Missing cell walls

Centre-cracked lattice specimens were manufactured with a row of missing cell walls at the centre of a regular lattice, see Fig. 2(b). The initial crack is of semi-length $a_0 = \sqrt{3}n_b\ell/2$ where n_b is the number of broken cell walls. The influence of crack length on the tensile strength of the lattice was explored by varying n_b between 0 and 6; three realisations of the lattice were generated for each value of n_b for the choice of $\bar{\rho} = 0.11$. Cell walls were removed before the test by locally heating up the cell walls by a soldering iron and struts were cut in the rubbery state of PMMA to prevent further cracking.

Figure 11(a) shows the measured tensile failure strength for the first strut failure (normalised by its corresponding mean value as measured for the regular lattice) as a function of the crack length a_0/ℓ . No knock-down in strength was found for $a_0/\ell \leq 3.5$. Therefore, the transition flaw size a_T is much larger compared to brittle lattices where the transition flaw size is in the order of one cell size and a significant drop in σ_f^∞ is observed when 1 or more struts are broken [13].

For long initial cracks ($a_0/\ell > 2.5$) struts near the introduced centre crack fail first (see Fig. 11(c)) and the following struts fail in the vicinity of the initial strut failure. Therefore, no diffusive failure was found in those samples. Close to the initial crack tip, vertical struts were found failing in the centre of the strut and not close to the nodes. The vertical struts fail under stretching as shown in the inset in Fig. 11(a).

7.3. Solid inclusions

Hexagonal lattices containing a solid inclusion were generated by the laser-cutting of PMMA sheets, with a number of intact filled cells at the centre of the specimen, recall Fig. 2(c). The semi-length of the inclusion is $a_0 = \sqrt{3}n_c\ell/2$ where n_c is the number of filled cells. Three realisations of the lattice were generated for each value of n_c between 0 and 6.

The measured values of macroscopic tensile strength σ_f^∞ are plotted in Fig. 11(b) as a function of the inclusion size a_0/ℓ , together for measured elastic-brittle results from Ref. [13]. It was found that filled cells of ductile materials lead to an increase of the strength with increasing a_0/ℓ . Elastic-brittle lattices do not show a distinct increase in strength with increasing inclusion size a_0/ℓ .

Ronan et al. [26] found that inclusions in lattices of elasto-plastic parent material reduce the lateral contraction of cells in the vicinity of the inclusions. In this case, struts fail by necking close to the inclusions. This is caused by the bi-axial stress state which is induced close to the inclusions. In the current study, strut necking was not found due to neck retardation of the visco-plastic parent material. Struts are drawn caused by the visco-plastic behaviour of PMMA near the solid inclusions (see inset in Fig. 11(b) and Fig. 11(d) for the case of $a_0/\ell = 2.6$) and fail at a high local axial failure strain due to the resistance to lateral cell contraction.

Inclusions do not promote a shift from a diffusive failure to a more correlated failure mode: struts fail with the same probability in the vicinity of the inclusion compared to struts in any other position. After diffusive strut failure occurred, one single crack was formed which might not be necessarily evolve close to the inclusions. This is also the case for the largest considered amount of solid inclusions in the samples ($a_0/\ell = 5.1$ which is equal to 6 filled cells).

In summary, lattices with filled cells showed a higher failure stress due to the reduced lateral contraction of cells in the vicinity of the inclusions. Therefore, filling cells could be used to enhance the tensile strength of ductile lattices.

8. Concluding remarks

The present study explores the sensitivity of the macroscopic tensile response of a visco-plastic lattice to as-manufactured and as-designed defects. It is found that both classes of defect have a significant effect on the macroscopic tensile strength of laser-cut PMMA lattices in the visco-plastic regime. FE analysis provides further insight into the relative potency of three types of as-manufactured defect: a dispersion in strut thickness, in Plateau border radius and in strut ductility arising from the manufacturing route.

The evolution of strut failure at T close to T_g is markedly different from that observed at ($T < T_g$) in a companion study, [13]. At room temperature, PMMA behaves in an elastic-brittle manner and the failure of a single strut is sufficient to induce the formation of a single macroscopic crack in the lattice. In contrast, at $T \approx T_g$, a diffuse zone of failed struts develop prior to catastrophic failure. Finite element analysis reveals that a dispersion in strut-to-strut ductility also plays a major role in the creep regime. A dispersion in ductility from

strut to strut is essential to give rise to the observed early onset of strut failure as well as the diffuse mode of fracture. Dispersion in strut thickness and Plateau border radius have only a mild effect in the visco-plastic regime, as confirmed by the FE predictions.

Imperfections were also introduced in the laser-cut lattices by design. Three kinds of imperfections were explored experimentally: randomly misplaced joints, a row of missing cell walls to create a notch, and a row of filled cells as solid inclusions. The following conclusions can be drawn for each type of defect:

- (i) *Imperfections in the form of randomly perturbed joints.* The macroscopic tensile strength of the lattice is sensitive to random perturbation of joints for low values of R/ℓ between 0 and 0.3. A 50% knockdown in tensile strength is observed when the imperfection is most severe ($R/\ell = 0.5$). The macroscopic ductility decreases with increasing values of R/ℓ due to formation of discrete force chains spanning the height of the specimen; a 40% reduction in the ductility is observed for $R/\ell = 0.5$. This behaviour is in contrast to brittle hexagonal lattices which are almost insensitive to randomly perturbed joints.
- (ii) *Imperfections in the form of missing cell walls.* Visco-plastic lattices possess high damage tolerance. The transition flaw size a_T for strength-controlled failure to fracture toughness-controlled failure is high such that the macroscopic tensile strength is not reduced even with 4 missing cells. This observation is consistent with the numerical predictions of Tankasala et al. [24] for a_T of ductile hexagonal lattices.
- (iii) *Imperfections in the form of solid inclusions.* The lattice tensile strength is insensitive to the presence of filled cells; no distinct knockdown in strength is observed for an inclusion size a_0/ℓ between 0 and 5.1. Lattices with filled cells showed an increased tensile strength due to the reduced lateral contraction of cells in the vicinity of the inclusions. Therefore, this effect could be used to enhance the tensile strength of ductile or visco-plastic lattices.

In summary, the macroscopic tensile strength of the visco-plastic hexagonal PMMA lattice is almost insensitive to imperfections in the form of broken cell walls and solid inclusions owing to its high transition flaw size. The random misplacement of joints emerges as the most potent type of defect.

Acknowledgements

The authors gratefully acknowledge the financial support from the European Research Council (ERC) under the European Union's Horizon 2020 research and innovation program, grant GA669764, MULTILAT.

References

- [1] L. J. Gibson, M. F. Ashby, *Cellular solids: structure and properties*, Cambridge university press, 1999.
- [2] E. W. Andrews, L. J. Gibson, M. F. Ashby, The creep of cellular solids, *Acta materialia* 47 (10) (1999) 2853–2863.
- [3] S. M. Oppenheimer, D. C. Dunand, Finite element modeling of creep deformation in cellular metals, *Acta Materialia* 55 (11) (2007) 3825–3834.
- [4] N. J. Mills, A. Gilchrist, Creep and recovery of polyolefin foams-deformation mechanisms, *Journal of cellular plastics* 33 (3) (1997) 264–292.
- [5] S. Deschanel, L. Vanel, N. Godin, E. Maire, G. Vigier, S. Ciliberto, Mechanical response and fracture dynamics of polymeric foams, *Journal of Physics D: Applied Physics* 42 (21) (2009) 214001.
- [6] H. X. Zhu, N. J. Mills, Modelling the creep of open-cell polymer foams, *Journal of the Mechanics and Physics of Solids* 47 (7) (1999) 1437–1457.
- [7] Z. G. Fan, C. Q. Chen, T. J. Lu, Multiaxial creep of low density open-cell foams, *Materials Science and Engineering: A* 540 (2012) 83–88.
- [8] K. A. Khan, R. K. A. Al-Rub, Time dependent response of architected Neovius foams, *International Journal of Mechanical Sciences* 126 (2017) 106–119.
- [9] J. S. Huang, L. J. Gibson, Creep of polymer foams, *Journal of materials science* 26 (3) (1991) 637–647.
- [10] J. S. Huang, L. J. Gibson, Creep of open-cell Voronoi foams, *Materials Science and Engineering: A* 339 (1-2) (2003) 220–226.
- [11] K. C. Goretta, R. Brezny, C. Q. Dam, D. J. Green, A. R. D. Arellano-Lopez, A. Dominguez-Rodriguez, High temperature mechanical behavior of porous open-cell Al₂O₃, *Materials Science and Engineering: A* 124 (2) (1990) 151–158.
- [12] T.-J. Chen, J.-S. Huang, Creep-rupturing of cellular materials: Regular hexagonal honeycombs with dual imperfections, *Composites Science and Technology* 68 (6) (2008) 1562–1569.
- [13] P. E. Seiler, H. C. Tankasala, N. A. Fleck, The role of defects in brittle honeycombs made via rapid prototyping, *Acta Materialia* 171 (2019) 190–200.
- [14] D. N. Boccaccini, H. L. Frandsen, B. R. Sudireddy, P. Blennow, Å. H. Persson, K. Kwok, P. V. Hendriksen, Creep behaviour of porous metal supports for solid oxide fuel cells, *international journal of hydrogen energy* 39 (36) (2014) 21569–21580.
- [15] B. Su, Z. Zhou, Z. Wang, Z. Li, X. Shu, Effect of defects on creep behavior of cellular materials, *Materials Letters* 136 (2014) 37–40.
- [16] B. Han, R.-P. Yu, Q.-C. Zhang, H.-J. Gao, Q. Zhang, T. J. Lu, B.-H. Lu, Creep of closed-cell aluminum foams: Effects of imperfections and predictive modeling, *Materials & Design* 156 (2018) 229–241.

- [17] J.-Y. Lin, J.-S. Huang, Creep of hexagonal honeycombs with Plateau borders, *Composite structures* 67 (4) (2005) 477–484.
- [18] F. Van Loock, N. A. Fleck, Deformation and failure maps for PMMA in uniaxial tension, *Polymer* 148 (2018) 259–268.
- [19] G. R. Johnson, W. H. Cook, Fracture Characteristics of Three Metals Subjected to Various Strains, Strain rates, Temperatures and Pressures, *Engg. Frac. Mech.* 21 (1) (1985) 31–48.
- [20] S. R. Choi, J. A. Salem, Fracture toughness of PMMA as measured with indentation cracks, *Journal of Materials Research* 8 (12) (1993) 3210–3217.
- [21] J. Oliver, A consistent characteristic length for smeared cracking models., *International Journal for Numerical Methods in Engineering* 28 (1989) 461–474.
- [22] N. A. Fleck, X. Qiu, The damage tolerance of elastic–brittle, two-dimensional isotropic lattices, *Journal of the Mechanics and Physics of Solids* 55 (3) (2007) 562–588.
- [23] I. Quintana-Alonso, S. P. Mai, N. A. Fleck, D. C. H. Oakes, M. V. Twigg, The fracture toughness of a cordierite square lattice, *Acta Materialia* 58 (1) (2010) 201–207.
- [24] H. C. Tankasala, V. S. Deshpande, N. A. Fleck, Tensile response of elastoplastic lattices at finite strain, *Journal of the Mechanics and Physics of Solids* 109 (2017) 307 – 330.
- [25] N. E. R. Romijn, N. A. Fleck, The fracture toughness of planar lattices: Imperfection sensitivity, *Journal of the Mechanics and Physics of Solids* 55 (12) (2007) 2538–2564.
- [26] W. Ronan, V. S. Deshpande, N. A. Fleck, The tensile ductility of cellular Solids: The role of imperfections, *International Journal of Solids and Structures* 102-103 (2016) 200–213.

Figures

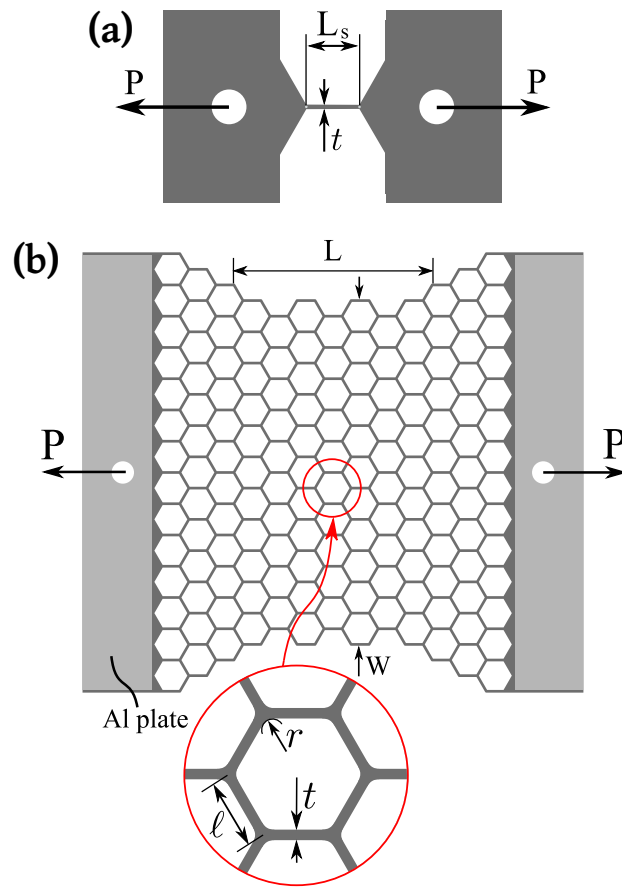


Figure 1: (a) Single strut specimen, and (b) regular lattice specimen of $\bar{\rho} = 0.11$. The sheet thickness of all samples is $B_0 = 5$ mm.

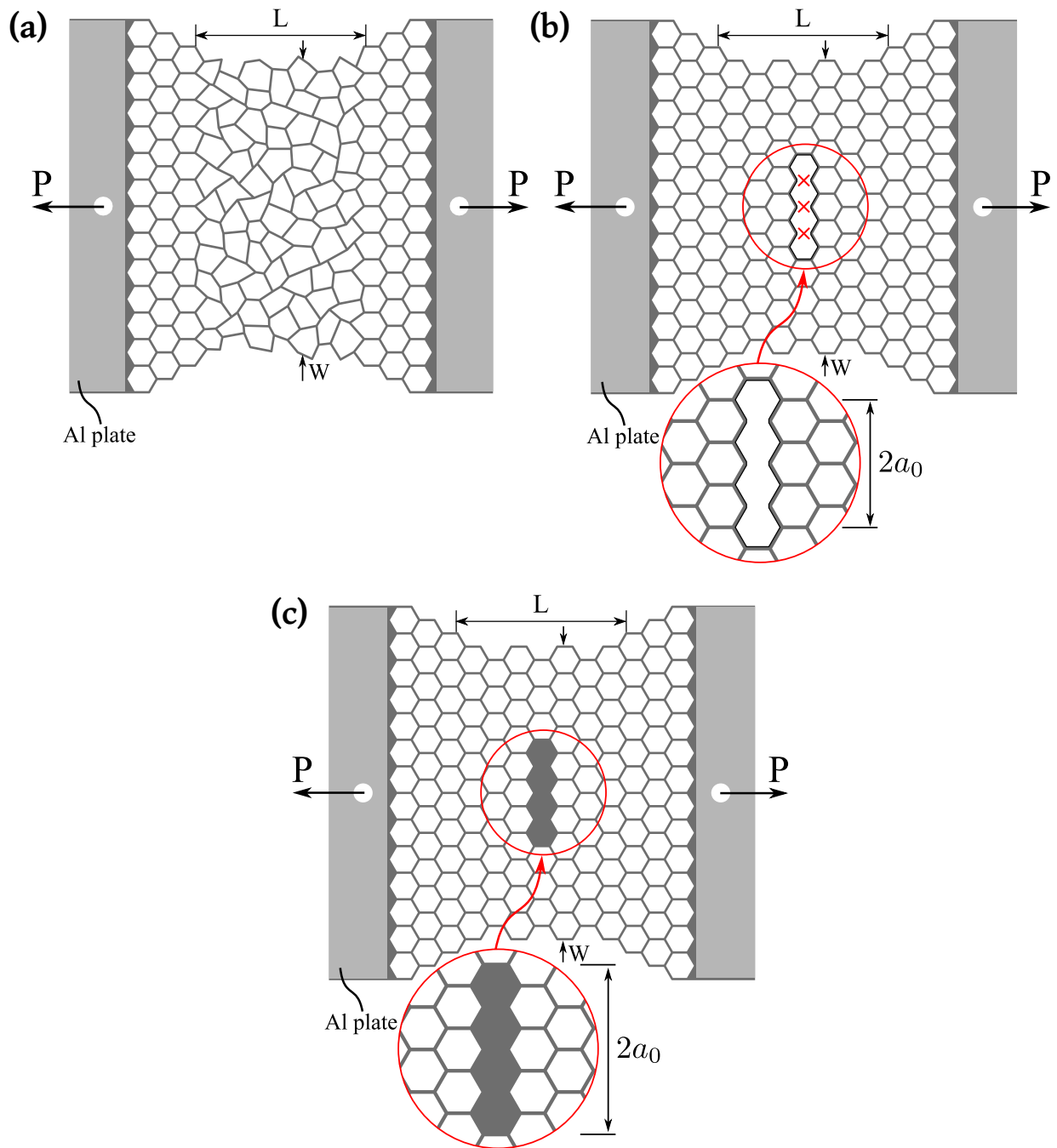


Figure 2: Lattice specimens ($\bar{\rho} = 0.11$) containing as-designed defects in the form of (a) randomly perturbed joints ($R/\ell = 0.5$), (b) a row of missing cell walls, and (c) a row of solid inclusions.

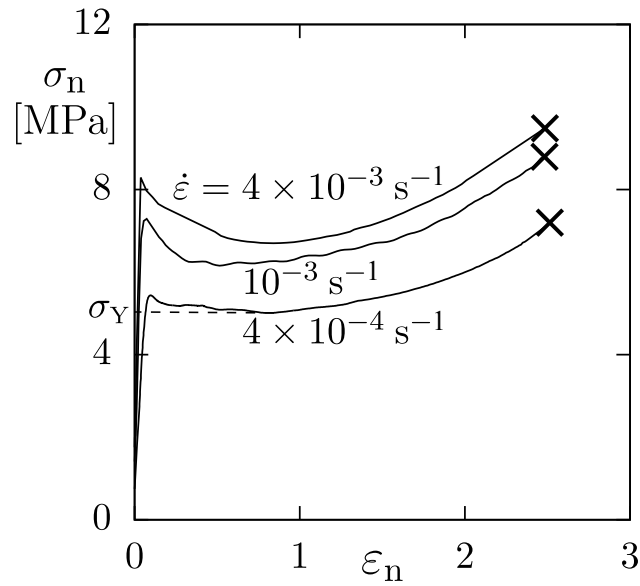


Figure 3: Nominal stress versus nominal strain response of single strut samples at 100 °C with varied strain-rate between $4 \times 10^{-4} \text{ s}^{-1}$ and $4 \times 10^{-3} \text{ s}^{-1}$.

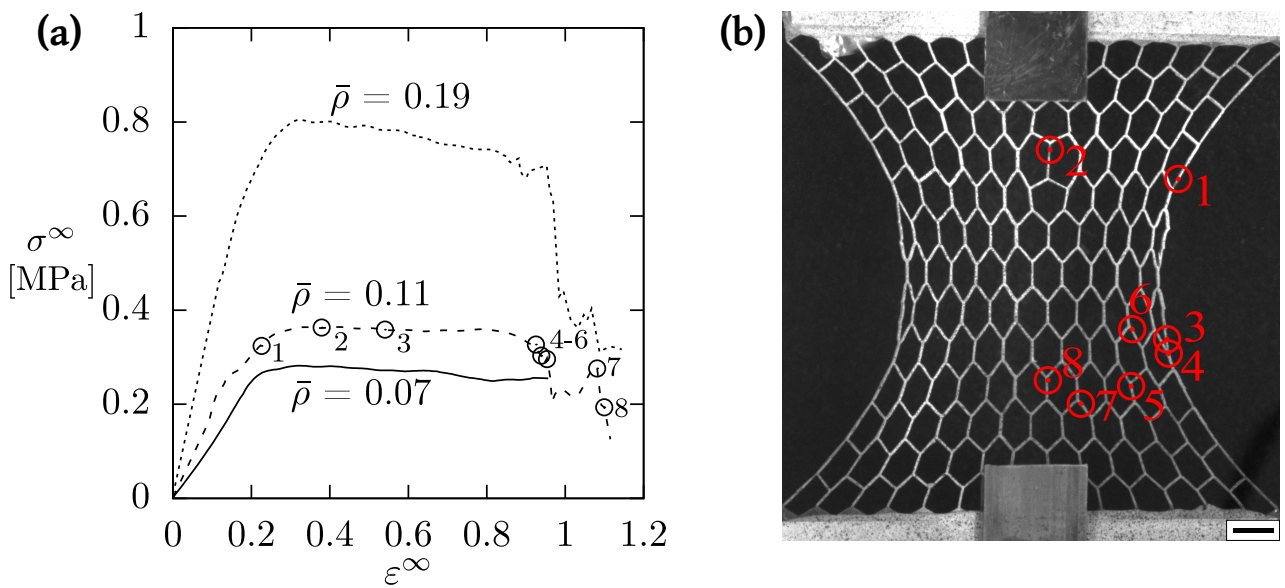


Figure 4: (a) Measured macroscopic stress versus strain response of regular lattices for selected values of relative density $\bar{\rho}$, (b) deformed regular lattice ($\bar{\rho} = 0.11$) before first strut failure (circles mark subsequent strut failure). The scale bar is of length 10 mm.

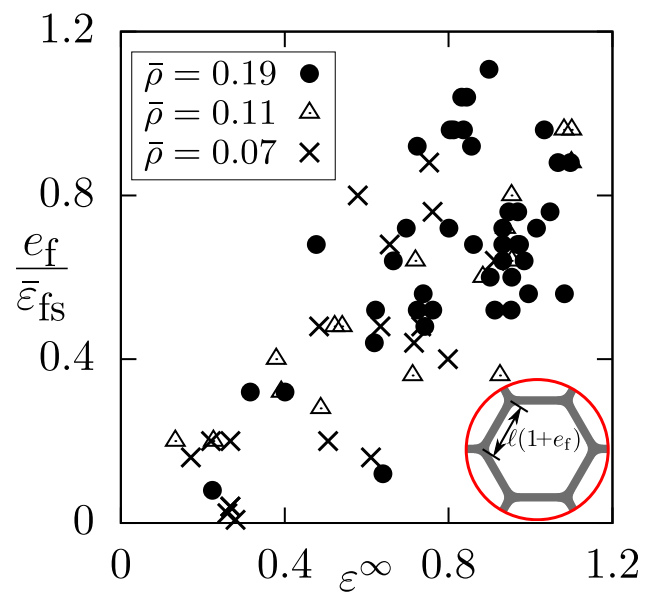


Figure 5: Measured axial failure strain of struts e_f versus the remote strain ϵ^∞ .

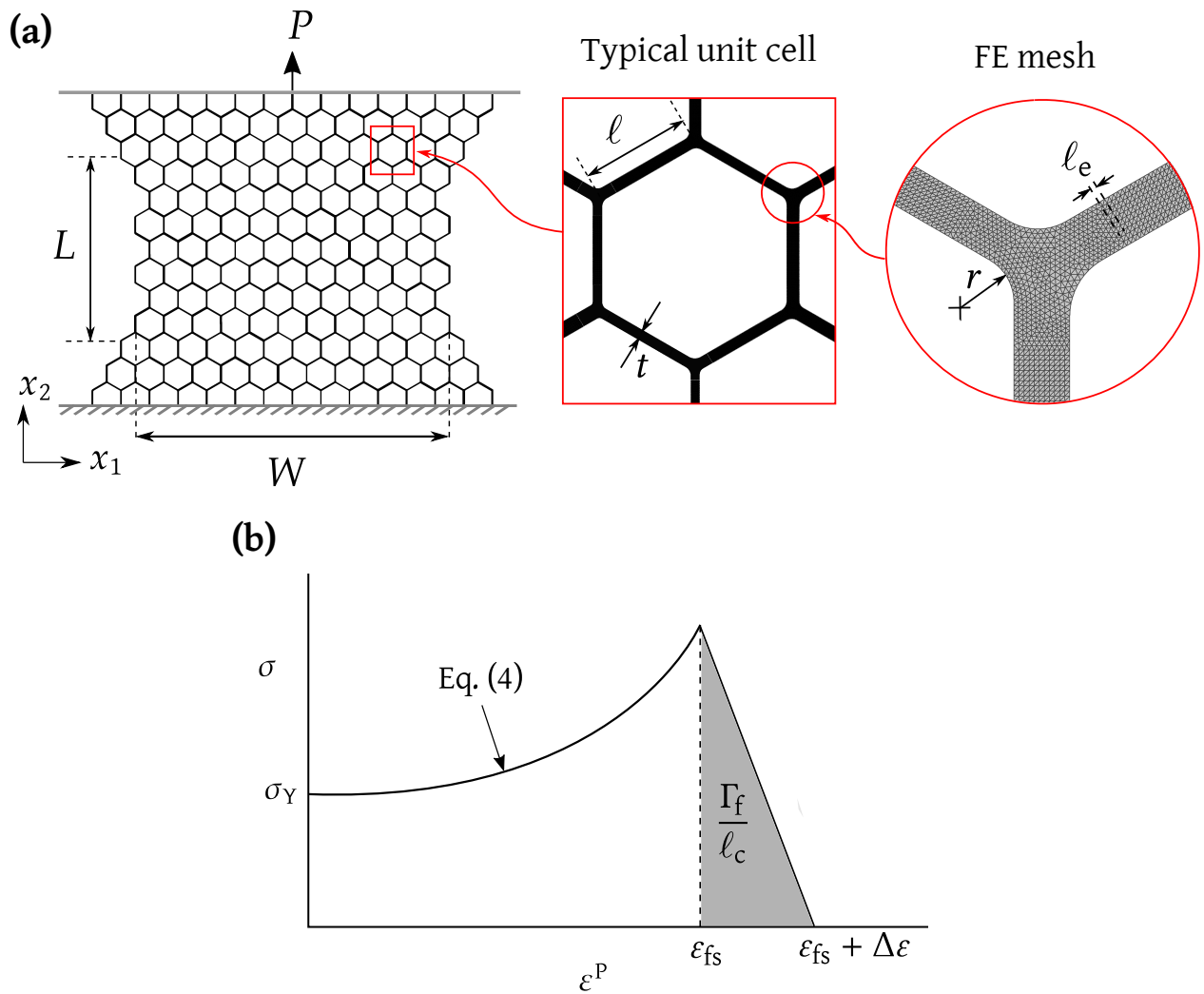


Figure 6: Details of the FE model: (a) geometry, loading, and boundary conditions employed in the FE simulations of lattice specimens under uniaxial tension. A typical unit cell within the lattice is shown along with the FE mesh for a joint. (b) Assumed stress versus strain response of the cell wall solid for one value of strain rate $\dot{\epsilon}$.

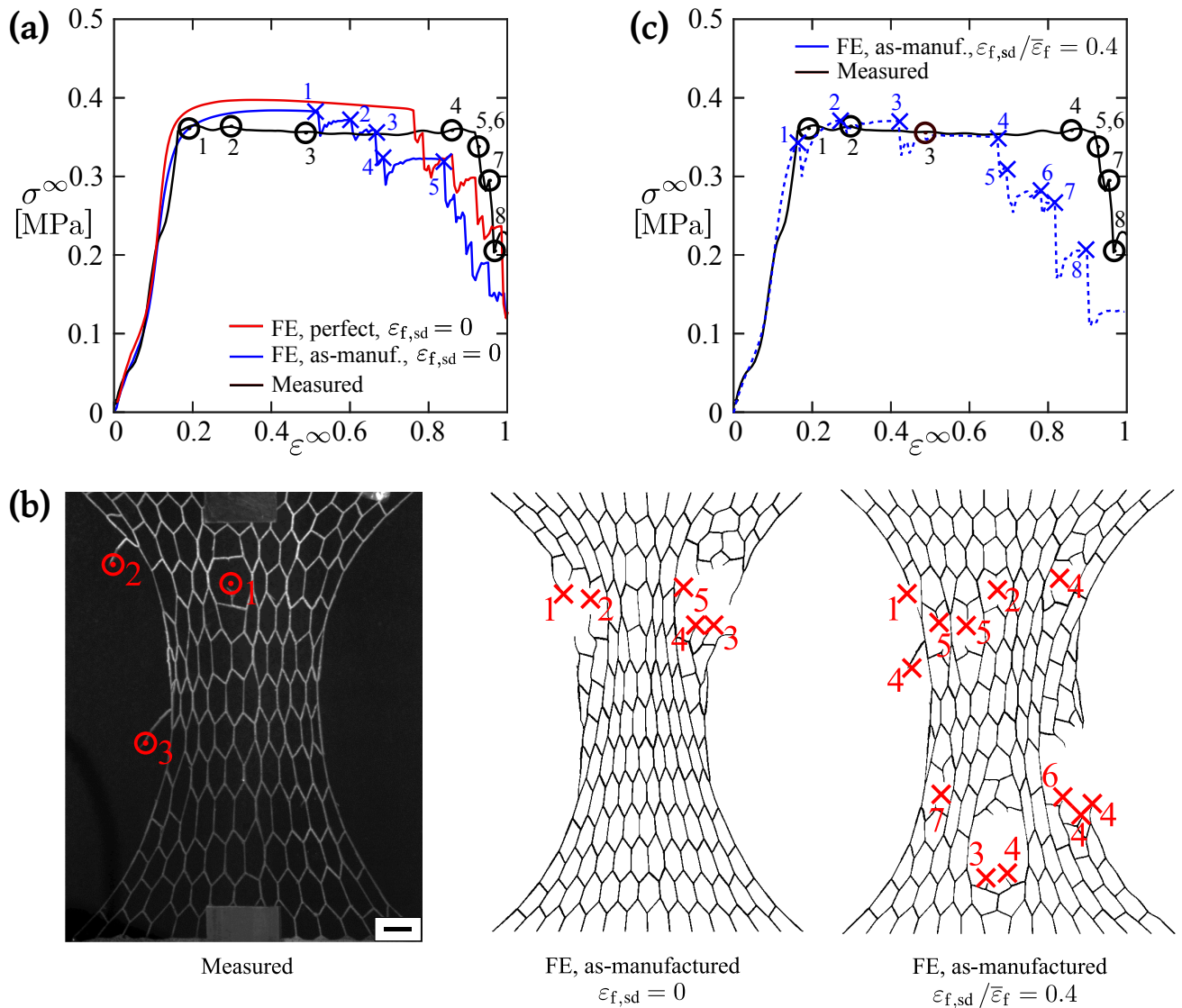


Figure 7: Measured versus predicted response for a lattice of relative density $\bar{\rho} = 0.11$: (a) macroscopic nominal stress σ^∞ versus macroscopic nominal strain of perfect lattices (FE) and as-manufactured geometries (FE and measured); (b) sequence of strut failure at $\epsilon^\infty = 0.8$ (circles: failed struts in experiment; crosses: predicted failed struts by FE); (c) macroscopic nominal stress σ^∞ versus macroscopic nominal strain with dispersion in strut ductility (FE) and measured. The scale bar is 10 mm.

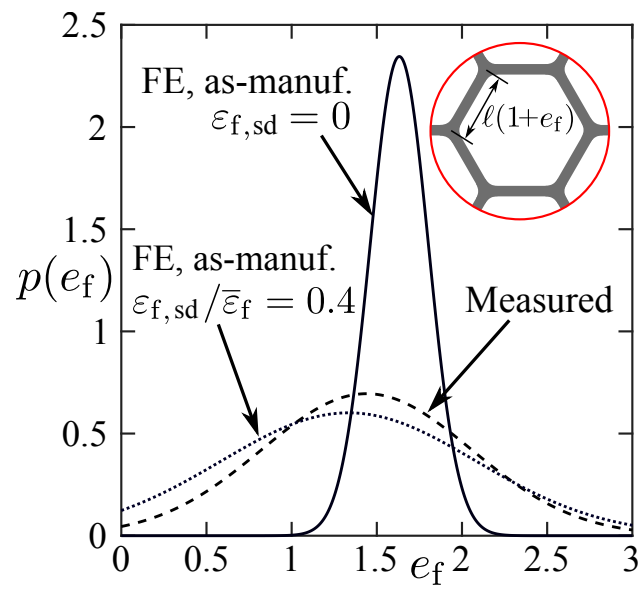


Figure 8: The probability distribution function $p(e_f)$ of the average strut ductility e_f for a lattice of relative density $\bar{\rho} = 0.11$.

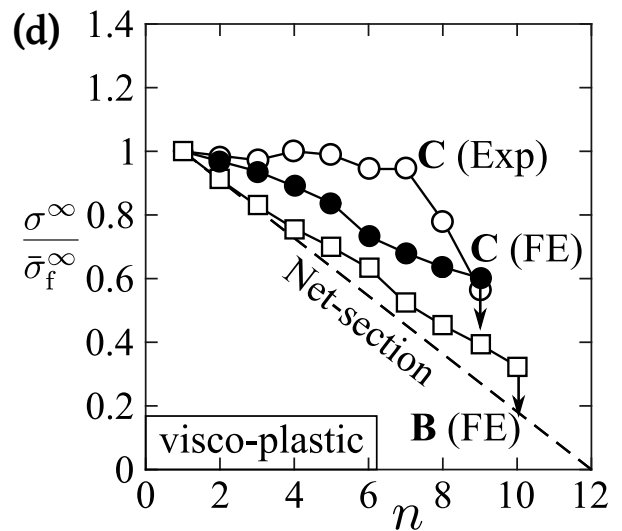
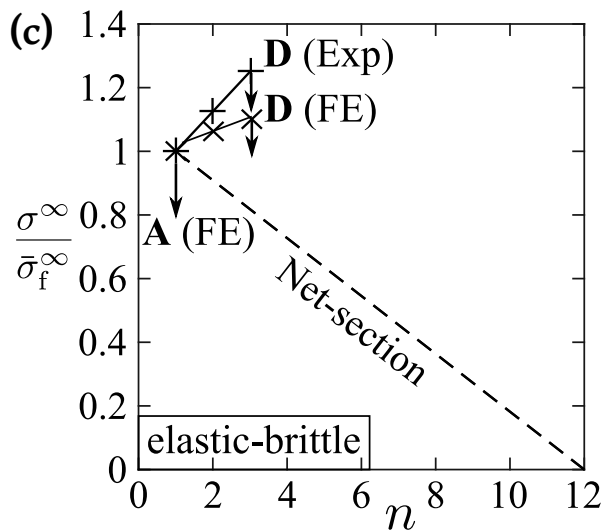
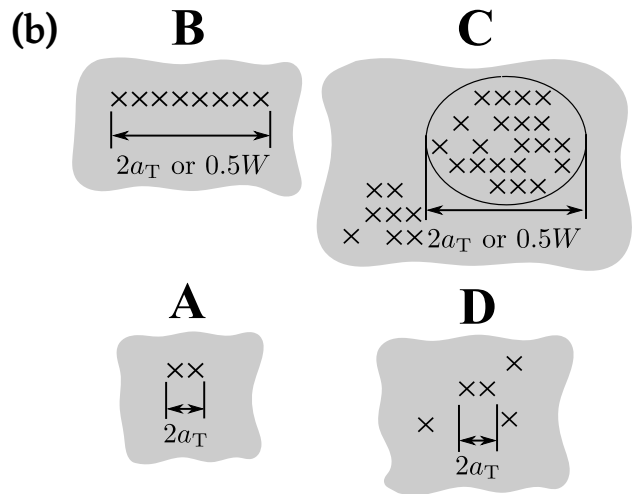
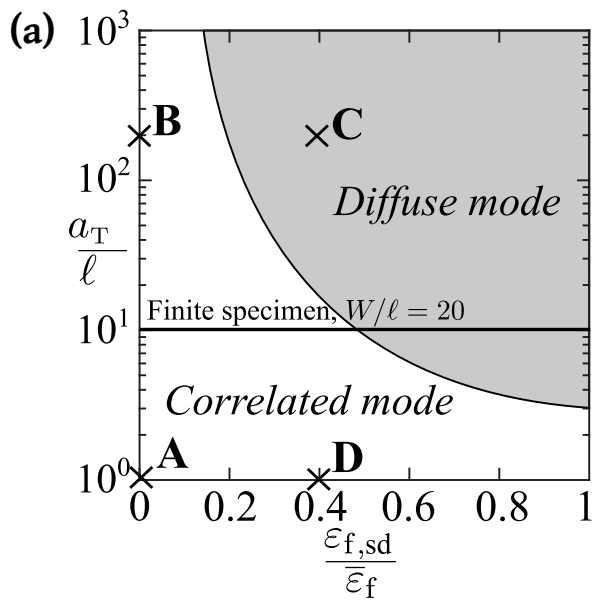
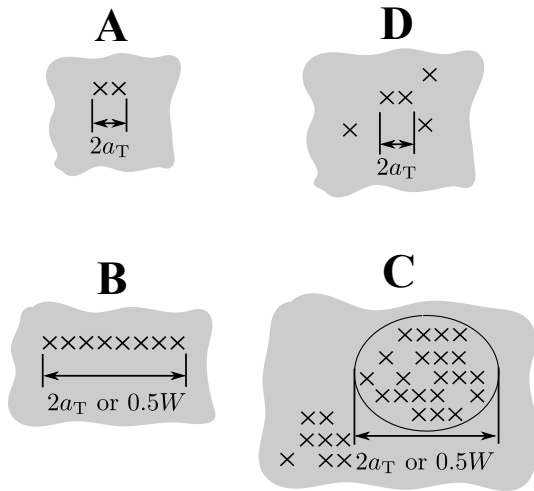


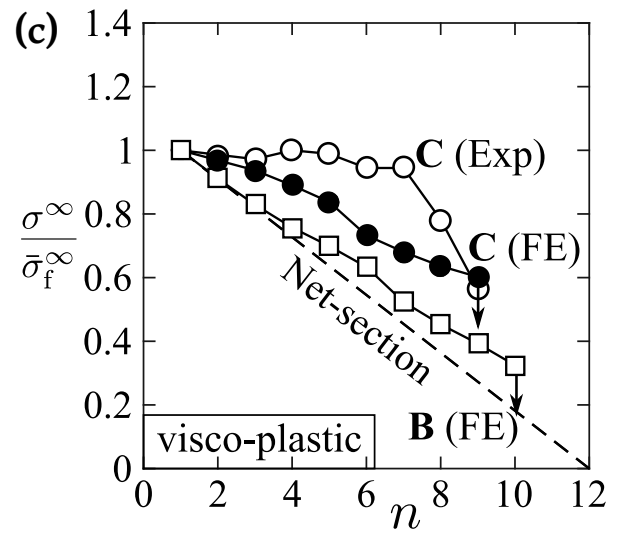
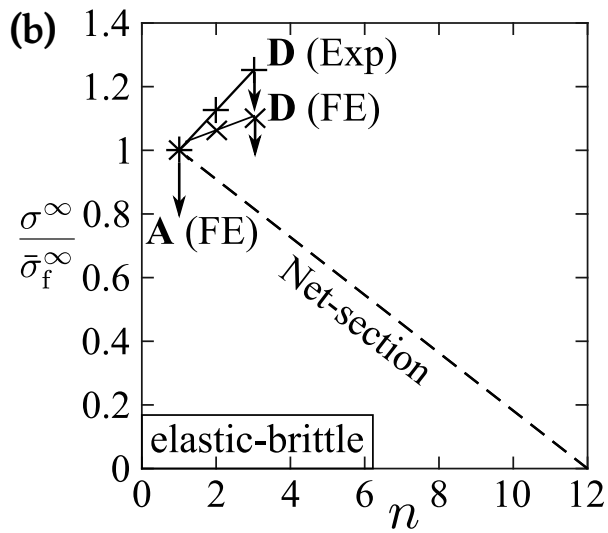
Figure 9: Correlated versus diffuse damage: (a) Map showing the parameter space for correlated versus diffuse modes of damage as a function of transition flaw size a_T/ℓ and the dispersion in material ductility $\varepsilon_{f,sd}/\bar{\varepsilon}_f$, and (a) a schematic of damage state at onset of fast fracture for cases A through D as labelled in (a). (b) The predicted and measured knockdown in macroscopic stress due to progressive failure of struts for cases A and D and (c) for cases B and C. These results correspond to a lattice of $\bar{\rho} = 0.11$.

(a)

NEW FIGURE 9



Case	$\frac{\varepsilon_{fs,sd}}{\bar{\varepsilon}_{fs}}$	$\min\left(\frac{2a_T}{\ell}, 0.5W\right)$	Mode of damage
A	0	$\frac{2a_T}{\ell}$	Correlated (FE)
B	0	$0.5W$	Correlated (FE)
C	0.4	$0.5W$	Diffuse (Expt. and FE)
D	0.4	$\frac{2a_T}{\ell}$	Correlated (Expt. and FE)



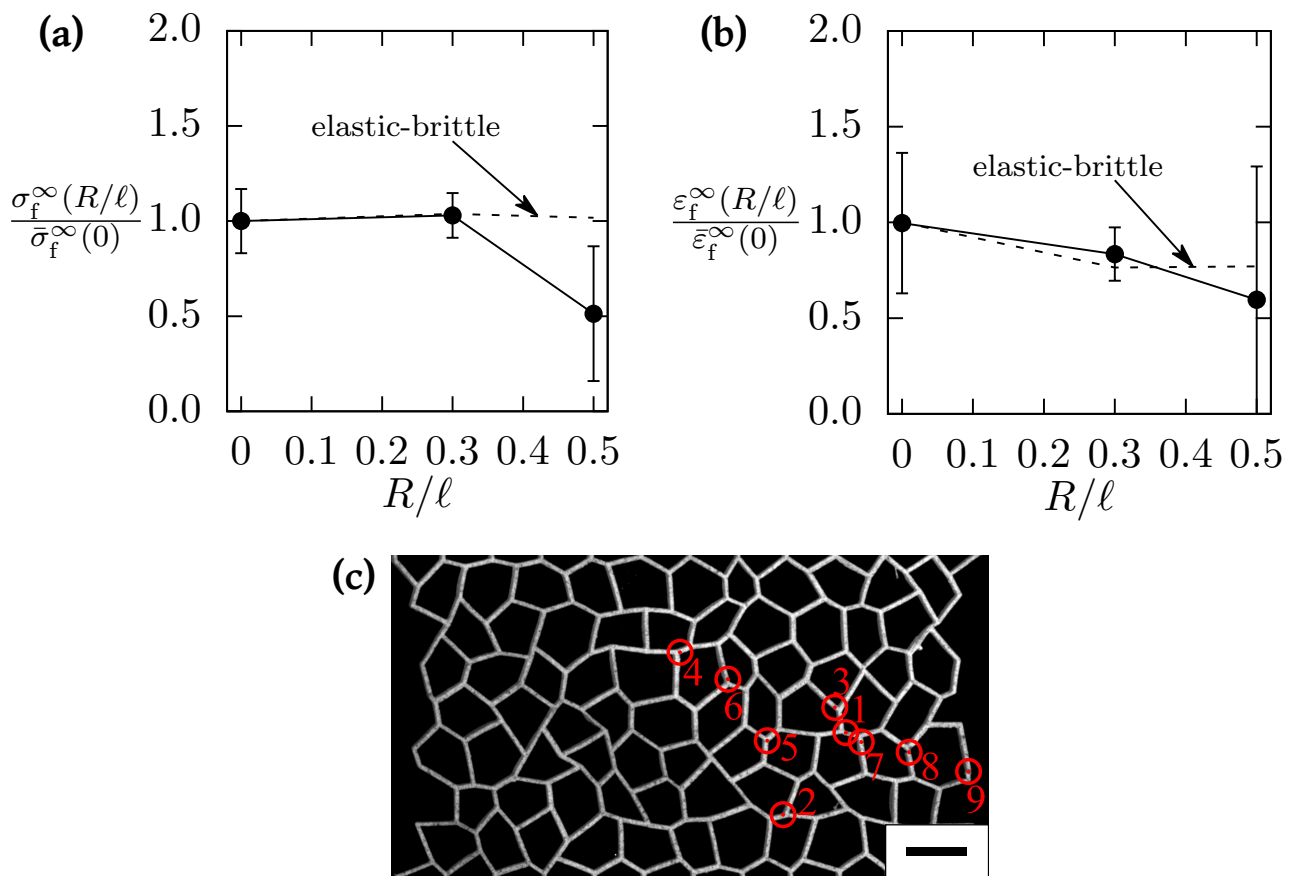


Figure 10: Measured macroscopic properties of imperfect lattices with randomly misplaced joints (including the measured elastic-brittle response from Seiler et al. [13]): (a) tensile failure stress σ_f^∞ and (b) tensile failure strain ε_f^∞ of first strut failure. (c) Sequence of strut failure for one specimen of ($R/\ell = 0.5$). The scale bar is of length 10 mm.

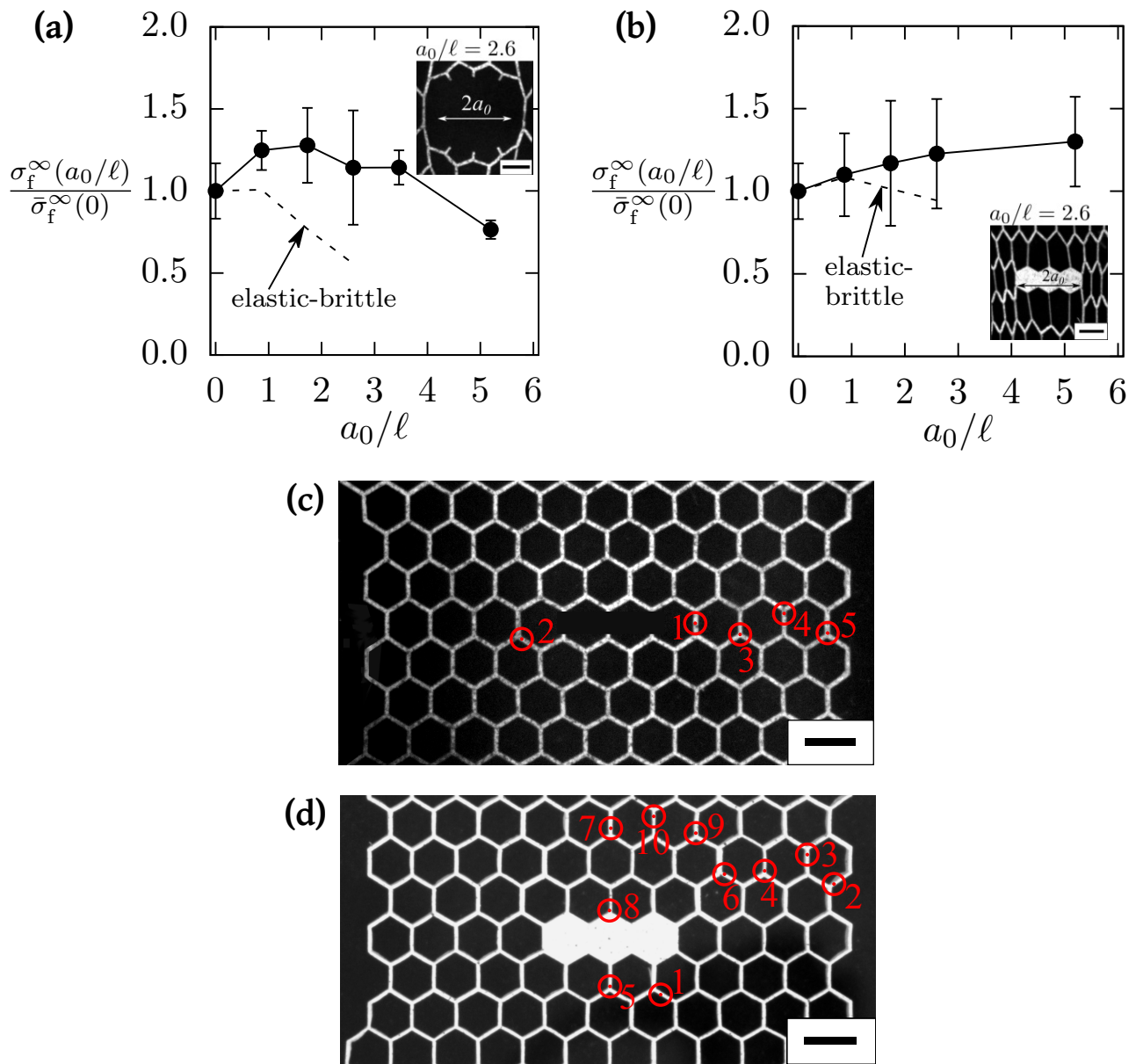


Figure 11: Measured tensile strength of lattice specimens (including the measured elastic-brittle response from Seiler et al. [13]) with (a) a row of missing cell walls and (b) a row of solid inclusions, as a function of the defect size a_0/ℓ . Stretched struts close to the as-designed imperfections before first strut failure are shown in the insets. Sequence of strut failure in one specimen containing (c) missing cell walls ($a_0/\ell = 2.6$) or (d) solid inclusion ($a_0/\ell = 2.6$). The scale bar is of length 10 mm.